JOURNAL OF MATERIALS SCIENCE 22 (1987) 137–143

Superplasticity of aluminium alloys grain-refined by zirconium

A. JUHÁSZ, N. Q. CHINH, P. TASNÁDI, I. KOVÁCS
Institute for General Physics, Loránd Eötvös University, Budapest, Hungary
T. TURMEZEY
HUNGALU Engineering and Development Centre, Budapest, Hungary

The superplasticity of aluminium alloys containing magnesium, zinc, iron and manganese as well as zirconium as a grain-refining addition element was investigated by high-temperature tensile tests. The total elongation and the strain rate sensitivity as a function of strain rate and temperature were determined. The activation enthalpy and activation volume were also determined in the superplastic region of the deformation. In addition to the tensile tests metallographic investigations were also made. The results obtained show that the superplasticity of the alloys investigated is increasing by the addition of iron but it is decreasing by the simultaneous addition of iron and manganese.

1. Introduction

There is a wide interest at present in the properties of superplastic alloys, mainly because of the possibility of forming products with complex shapes using relatively inexpensive tooling.

The purpose of this paper is to report the results of laboratory experiments which demonstrate that Al–Zn–Mg alloys close in composition to that produced commercially can be made to exhibit superplasticity by the addition of zirconium as a grain-refining element.

The superplastic properties of Al–Cu and Al–Cu–Zr alloys are well documented [1, 2]. Grimes *et al.* [1] used zinc as a substitute for copper because zinc is one of the few alloying elements which is soluble in a significant amount in aluminium.

There are two basic requirements for achieving superplasticity. First it is necessary to produce a very fine-grained material, and secondly, the grain size and structure have to be relatively stable.

The first requirement can be fulfilled by the addition of zirconium which has a grain-refining effect in Al–Zn–Mg alloys. This effect is probably caused by the metastable phase particles of Al_3Zr which can act as nuclei of new grains [3].

There are only a few papers in the literature dealing with the superplasticity of Al–Zn–Mg–Zr alloys. In a recent review Gittus [4] deals with these alloys only on the basis of the article of Grimes *et al.* [1]. More recently Shakesheff and Partridge [5] investigated the superplasticity of an Al–6.2 Zn–2.5 Mg–1.7 Cu–0.4 Zr–0.11 Fe–0.07 Si alloy.

The aim of the present paper is to study the superplasticity of a set of Al–Zn–Mg alloys with different additional elements.

2. Experimental procedure

The chemical composition of the alloys investigated are given in Table I. The alloys were prepared from 99.99% purity aluminium by the HUNGALU Engineering and Development Centre, Budapest. The cast rods were warm-rolled into sheets of 2 mm thickness. The tensile specimens were cut parallel to the direction of rolling by spark-machining with a gauge length of 6.5 mm (Fig. 1). The tensile tests were carried out in an air furnace attached to an Instron machine. The samples were put into the furnace preheated previously and the test was begun after waiting about 20 to 30 min for reaching thermal equilibrium. During the tests the temperature of the furnace was controlled to $\pm 2°$ C. The temperature of the tensile testing was selected on the basis of recrystallization measurements. Such temperatures were chosen at which the alloys were progressively but not totally recrystallized during one hour of annealing. The tensile tests were conducted with a few different cross-head velocities, and usually two or three samples were investigated under the same conditions. The mean values of parallel measurements were used as the experimental data.

The stress–strain curves and the total elongation up to failure were determined on the basis of the force–elongation diagrams taken at different temperatures and strain rates. Strain rate sensitivities as a function of strain rate were calculated at different temperatures applying the strain rate change method [6]. The strain rate sensitivities of Sample 2 were determined from

TABLE I Compositions of alloys (balance Al)

Alloy	Composition (wt %)					
	Mg	Zn	Cu	Zr	Fe	Mn
1	–	–	5.8	0.5	–	–
2	0.98	4.6	–	0.5	–	–
3	0.98	4.65	–	0.49	0.15	–
4	1.04	4.8	–	0.51	0.15	0.34

0022–2461/87 $03.00 + .12

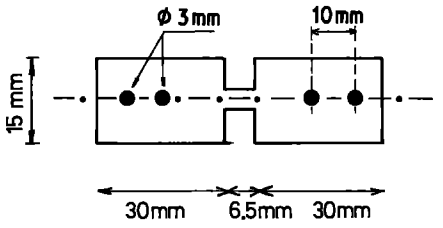

Figure 1 The tensile specimens.

stress relaxation measurements too. In the case of this material the strain rate sensitivity at a given strain rate was determined at different amounts of strain.

The changes of microstructure of the samples due to the deformation were followed by metallography. The samples were polished mechanically and electrolitically, and after that they were etched in a mixture of alcohol and perchloric acid. Optical micrographs were taken at the necked part of the samples, and for the sake of comparison some pictures were also taken at the undeformed parts of the samples.

3. Results

3.1. Stress–strain curves

A typical force–elongation curve of Sample 2 is shown in Fig. 2a. The stress–strain curve of Fig. 2b was calculated on the basis of these data, using the assumption that the volume of the sample is constant and the elongation is uniform in the course of the test. The variation of stress–strain curves with temperature and strain rate is shown in Figs 3 and 4, respectively.

3.2. Strain rate sensitivity parameter

In Fig. 5 the strain rate sensitivities obtained by stress relaxation measurements and by the strain rate change method at 500° C are plotted against the strain rate. It can be seen that the agreement between the strain rate sensitivities determined by the two methods is quite good. Fig. 6 shows that the strain rate sensitivity of Sample 2 at 500° C is independent of the strain. The strain rate sensitivity as a function of the strain rate

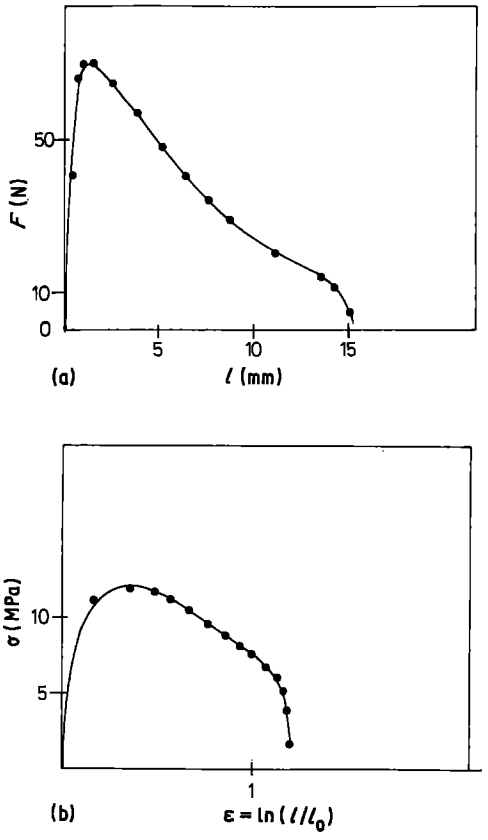

Figure 2 (a) Force–elongation curve and (b) true stress–true strain curve of Alloy 2. T = 500° C, cross-head velocity 2 mm min^{-1}.

is shown in Fig. 7 for the four different alloys at different temperatures. According to Fig. 7a, in the case of Alloy 2 the points lie along typical maximum curves. The highest maximum reaches 0.5 at 500° C and 555° C at $\dot{\varepsilon} = 5 \times 10^{-3}$ sec^{-1}. In the case of the other three alloys the strain rate sensitivity decreases monotonically with increasing strain rate (Figs 7b to d). For Alloy 4 the strain rate sensitivities are lower than those obtained for Alloys 2 and 3. In the case of Alloy 1 $m \leqslant 0.3$ everywhere in the range of temperature and strain rate investigated.

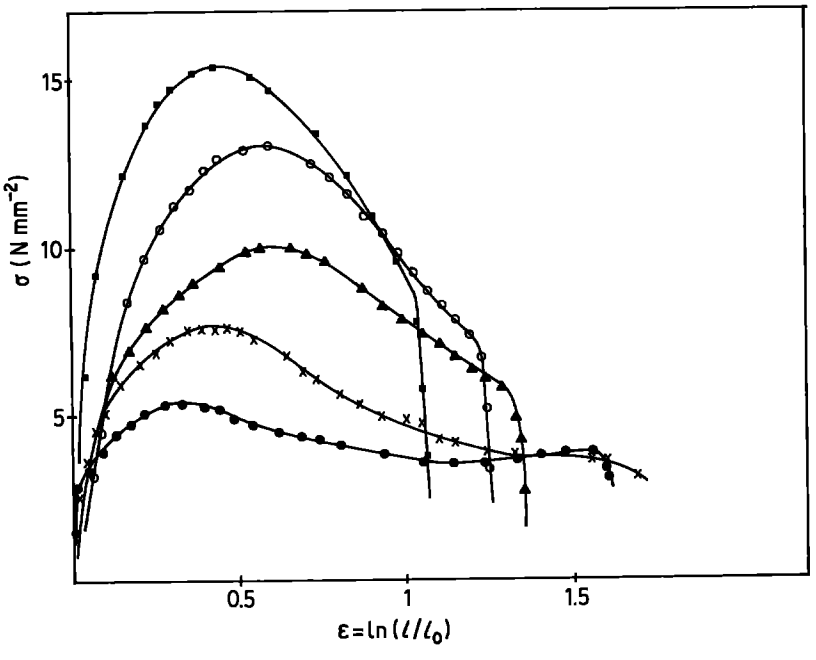

Figure 3 True stress–true strain curves of Alloy 3 at 500° C and different cross-head velocities: (●) 0.2, (x) 0.5, (▲) 1, (○) 2, (■) 3 mm sec^{-1}.

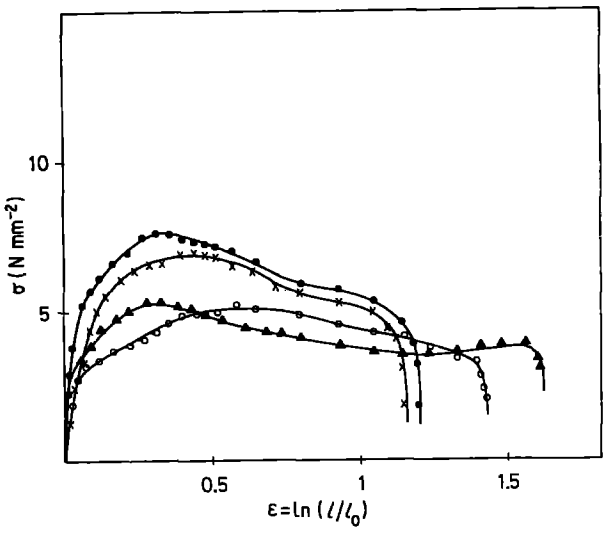

Figure 4 True stress–true strain curves of Alloy 3 at cross-head velocity 0.2 mm sec^{-1} and different temperatures: (●) 454, (x) 483, (▲) 500, (○) 525° C.

3.3. Total elongation

From the four alloys investigated only two show elongation higher than 200%. The highest elongation (450%) was measured on Alloy 3 at 3×10^{-4} sec^{-1} strain rate and at 500° C. The total elongation of Alloys 1 and 4 varied only slightly with temperature and strain rate and its magnitude was usually under 150%.

In order to show directly the relation between the total elongation and the strain rate sensitivity, a picture of the samples of Alloy 2 elongated maximally at a given strain rate is shown in Fig. 8, together with the plot of the corresponding m values. The connection between the total elongation and strain rate sensitivity of different alloys is shown in Fig. 9.

3.4. Structural changes during deformation

The initial structure of the alloys investigated was a typical rolled structure. On the optical micrographs, deformation bands parallel with the rolling direction could be observed but the grains could not be distinguished.

The microstructure of the samples is changing in the course of high-temperature deformation because the sample recrystallizes and voids and cavitations are formed. The voids and cavitations can be revealed by etching. (The surroundings of them have enhanced chemical activity, so dark spots appear on the metallographic pictures.)

In Fig. 10 the microstructure developed at 500° C after deformation at a cross-head velocity of 0.5 mm min^{-1} can be seen for Alloy 3. The picture in Fig. 10a was taken at a transverse section of a part of the sample deformed superplastically up to about 400%. Fig. 10b also shows a transversal section of a part of the sample, but the picture was taken at the undeformed part of the sample. In Fig. 11 three transversal sections of Sample 2 can be seen. The pictures taken after three different strains at a cross-head velocity of 1 mm min^{-1} and at 500° C show a continuous increase of the cavitations and also the grain coarsening during superplastic deformation.

4. Discussion

The stress–strain curves in Figs 3 and 4 are typical maximum curves. The stress reaches its maximum at about $\varepsilon = 0.3$ to 0.4 and after this it decreases monotonically. In a relatively large interval of strains the stress is a linear function of strain. The decrease of the stress is caused by the development of necks and cavitations with the progress of deformation; therefore the stress values given by the stress–strain curves characterize the real true stresses only up to the maximum of the elongation–force curves. Therefore the strain sensitivities were determined at lower strains than the one due to the stress maximum.

Similarly the calculation of the activation volume and the activation energy were based on the increasing parts of the stress–strain curves. The interpretation of the decreasing parts of the stress–strain curves will be discussed in a following paper.

Fig. 7 shows that the strain rate sensitivity is strongly dependent on temperature and strain rate and on material properties. It can be seen that the strain rate sensitivity of Alloy 2 is identical with those obtained for the well-known superplastic alloys with eutectic and eutectoid composition [7]. In Fig. 9 the connection between the total elongation and the strain

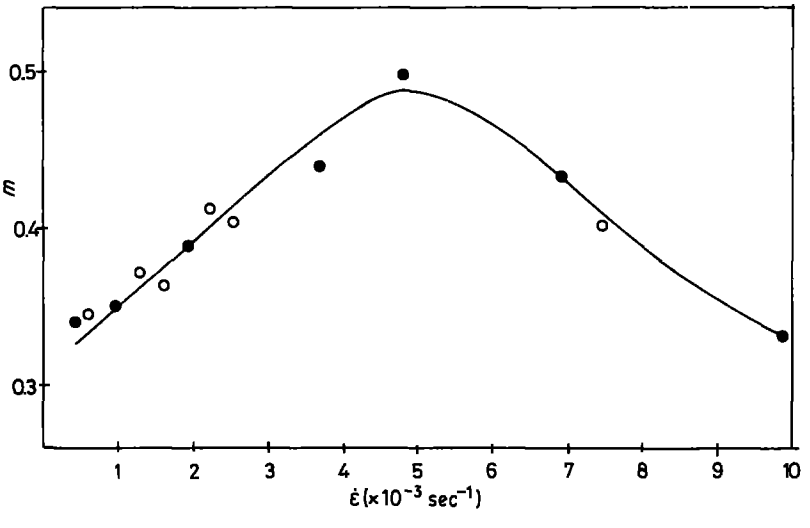

Figure 5 The strain rate sensitivity as a function of strain rate for Alloy 2 at 500° C: (●) strain rate change method, (○) stress relaxation method.

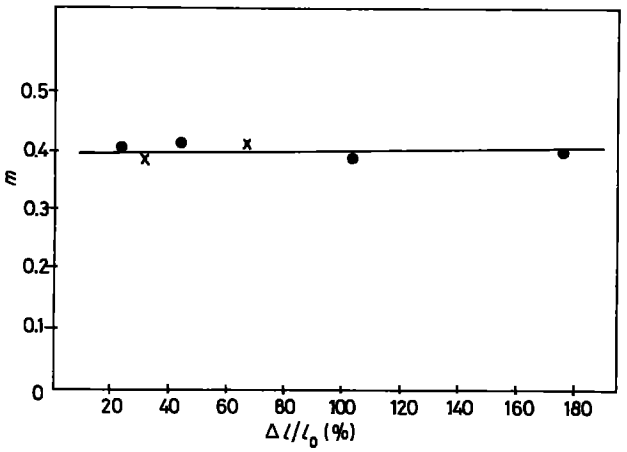

Figure 6 The strain rate sensitivity as a function of strain for Alloy 2 at 500° C: (●) stress relaxation method, (×) strain rate change method.

rate sensitivity is plotted. The result is in good agreement with previous results [8].

According to the total elongations and strain rate sensitivities measured, Alloys 2 and 3 can be considered as superplastic. Alloys 1 and 4, although they have a good ductility, do not show superplastic behaviour at least at reasonable strain rates. However, the strain rate sensitivities of Alloys 1, 3 and 4 are quite different; they decrease monotonically in the strain rate range investigated. For Alloy 2 made from a high-purity material the maximum m value was obtained at 450 to 550° C at a strain rate of the order of magnitude of 10^{-3} sec^{-1}. For Alloy 3 this maximum is due to a strain rate of about 10^{-4} sec^{-1}. It means that the optimal strain rate for superplastic forming of Alloy 3 is much lower than for Alloy 2. On the basis of the curves given in Fig. 7b to d one can suppose that these curves show only the final, decreasing part of the characteristic maximum curves. This conclusion is supported by the results of Shakesheff and Partridge [5]. They investigated the superplasticity of an alloy very similar in composition to Alloy 3, and the maximum m values were found in the strain rate range of 10^{-5} to 10^{-4} sec^{-1}.

4.1. The activation enthalpy

In the case of thermally activated deformation processes the relationship between strain rate $\dot{\varepsilon}$ and stress σ is usually given [9] by

$$\dot{\varepsilon} = C\sigma^{1/m}e^{-\Delta G/kT}$$

where m is the strain rate sensitivity parameter, ΔG the activation enthalpy and C is a constant.

If $\dot{\varepsilon}$ and m are kept constant then ΔG can be determined from the equation

$$\frac{1}{m}\ln\sigma = C^* + \frac{\Delta G}{kT}$$

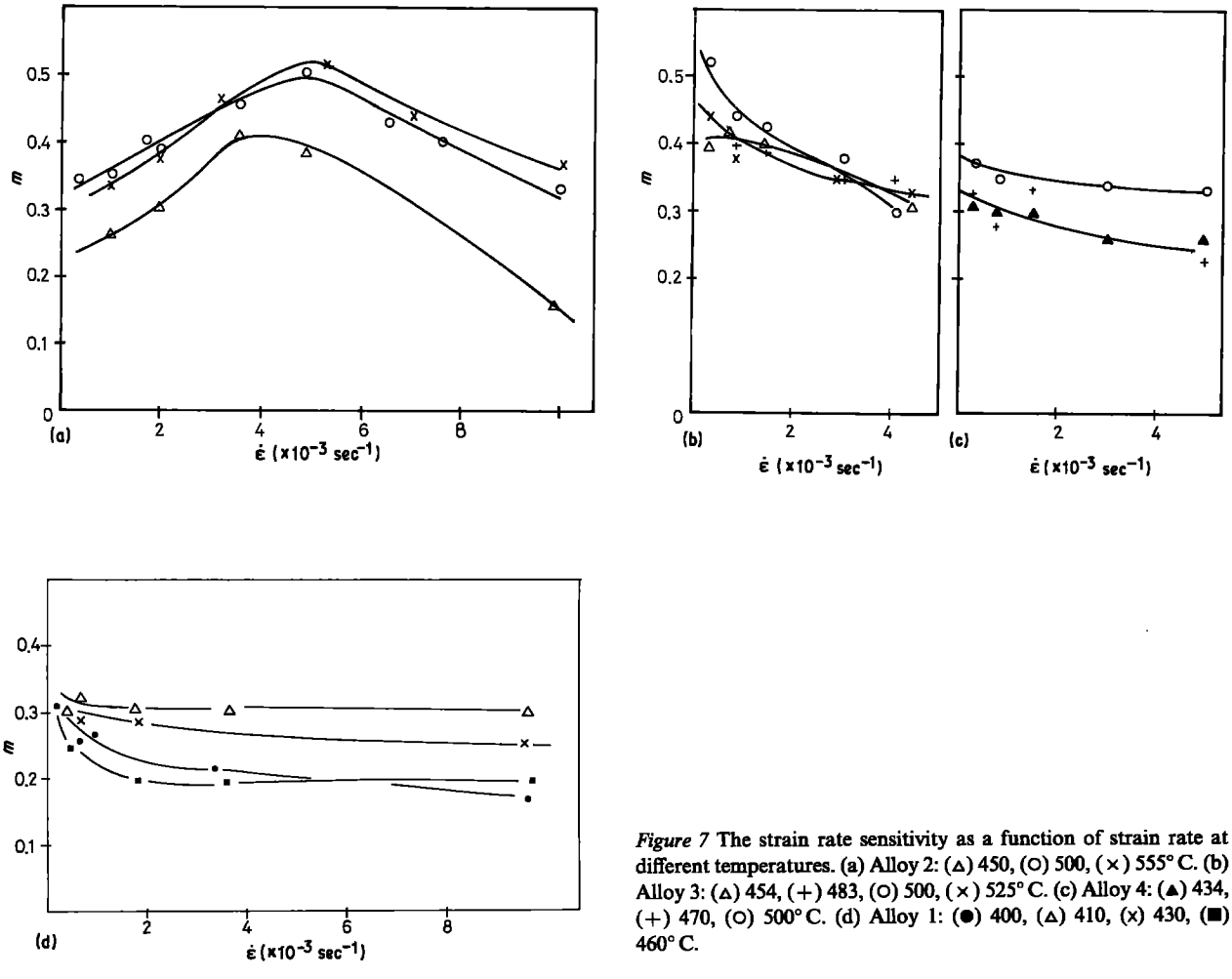

Figure 7 The strain rate sensitivity as a function of strain rate at different temperatures. (a) Alloy 2: (△) 450, (○) 500, (×) 555° C. (b) Alloy 3: (△) 454, (+) 483, (○) 500, (×) 525° C. (c) Alloy 4: (▲) 434, (+) 470, (○) 500° C. (d) Alloy 1: (●) 400, (△) 410, (x) 430, (■) 460° C.

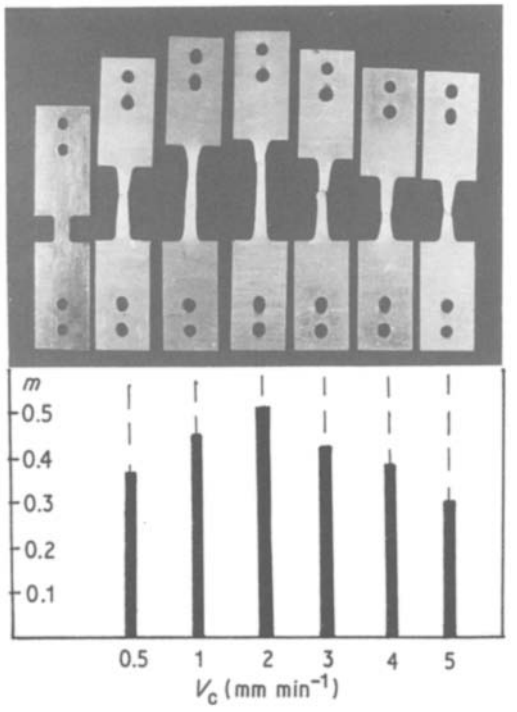

Figure 8 Maximally elongated samples and strain rate sensitivity.

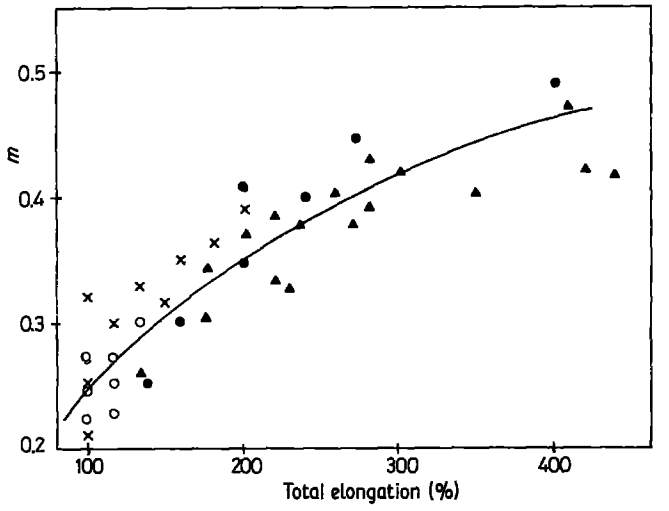

Figure 9 The strain rate sensitivity as a function of total elongation: (○) Alloy 1, (×) Alloy 2, (▲) Alloy 3, (●) Alloy 4.

where

$$C^* = \ln \frac{\dot{\varepsilon}}{C}$$

To determine the activation enthalpy, the data of those stress–strain curves were used which belong to the same strain rate sensitivities. From the curves chosen the activation enthalpy was obtained by the cross-cut method. In Fig. 12 the $\ln \sigma - 1/T$ function is shown for Alloy 2 in the case of three different strain rates at $m = 0.4$. An activation enthalpy of 0.75 eV was obtained from the slopes of the parallel straight lines.

In Fig. 13 the $\ln \sigma - 1/T$ curves are shown for Alloy 3. The strain rate sensitivity of this alloy is approximately 0.4 over a wide range of strain rate. The four lower curves of $\ln \sigma - 1/T$ are approximately parallel. The activation enthalpy obtained from these curves is $\Delta G = 0.67$ eV. In the case of the strain rate 4×10^{-4} sec^{-1} the activation enthalpy was found to be $\Delta G = 1.06$ eV, which is probably a consequence of the low strain rate sensitivity ($m \approx 0.31$) at this strain rate.

The ductility of the other two alloys is much smaller that that of the two discussed above. Their strain rate sensitivity lies between 0.2 and 0.3 and the points have a large scatter. Because of the uncertainty of the strain rate sensitivities the activation enthalpy can be estimated only rather roughly for these alloys. The activation enthalpy estimated was higher than 1.2 eV in both cases.

A comparision of the activation enthalpies obtained with self-diffusion enthalpy of aluminium (1.28 to 1.31 eV) indicates that the controlling mechanism of the superplastic deformation ($m \approx 0.4$) is grain-boundary sliding. Namely, the activation enthalpy of grain-boundary sliding is equal to the grain-boundary diffusion enthalpy which is about 50 to 75% of the self-diffusion enthalpy [10]. The greater activation enthalpies obtained in the case of samples with $m < 0.4$ show that deformation in these samples is probably controlled by self-diffusion.

4.2. The activation volume

Thermally activated plastic deformation can be

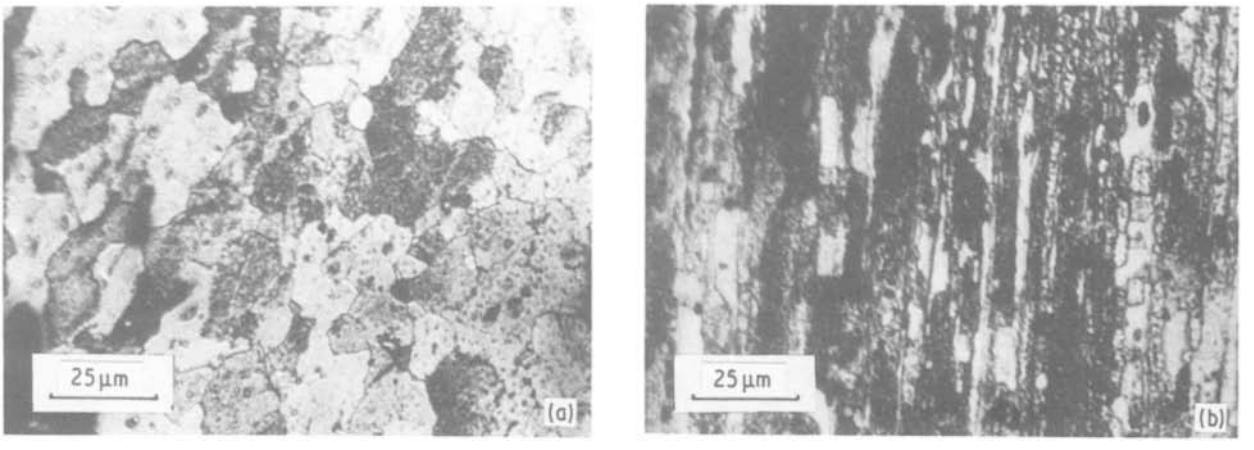

Figure 10 The microstructure of Alloy 3: (a) the deformed part of the sample, (b) the undeformed part of the sample.

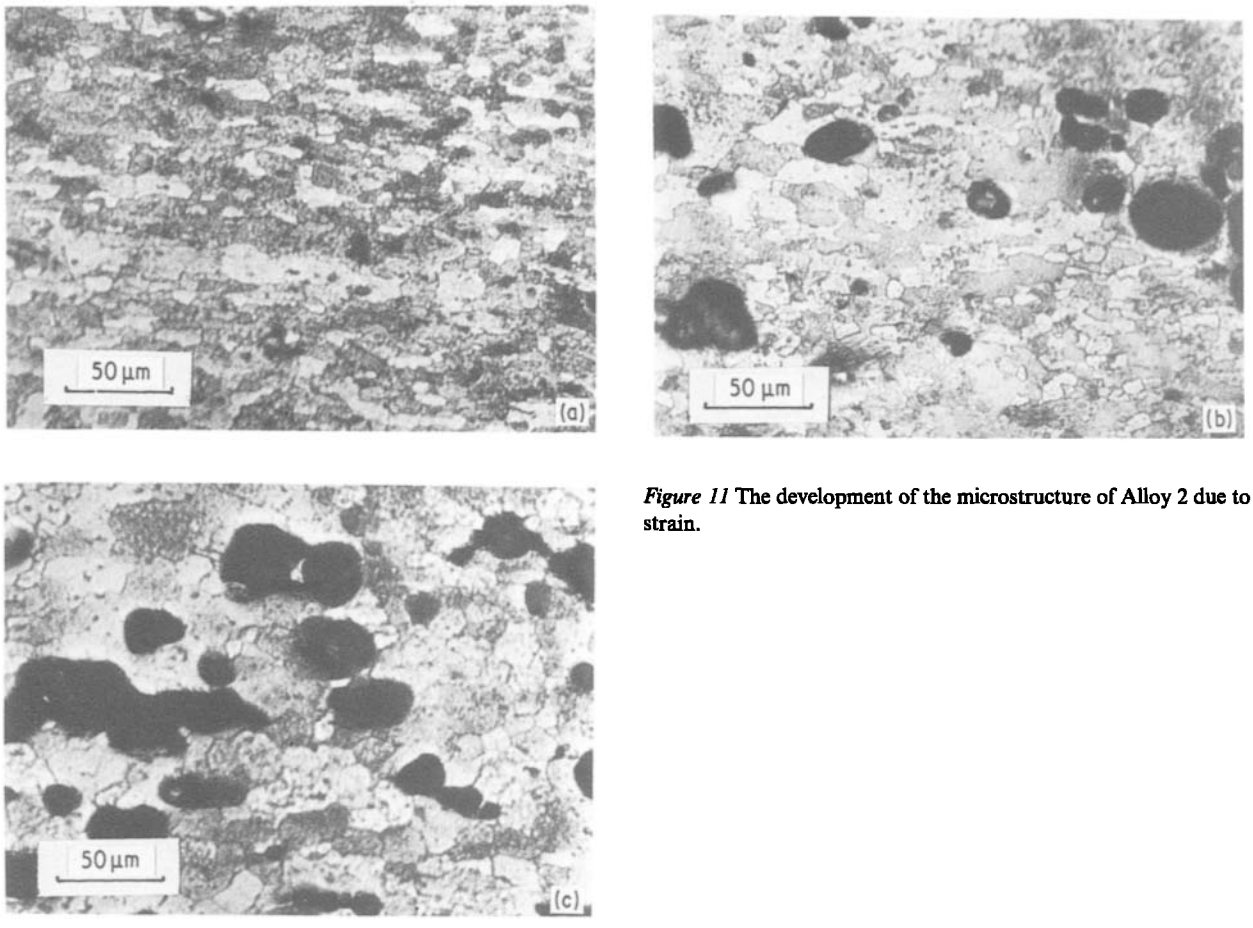

Figure 11 The development of the microstructure of Alloy 2 due to strain.

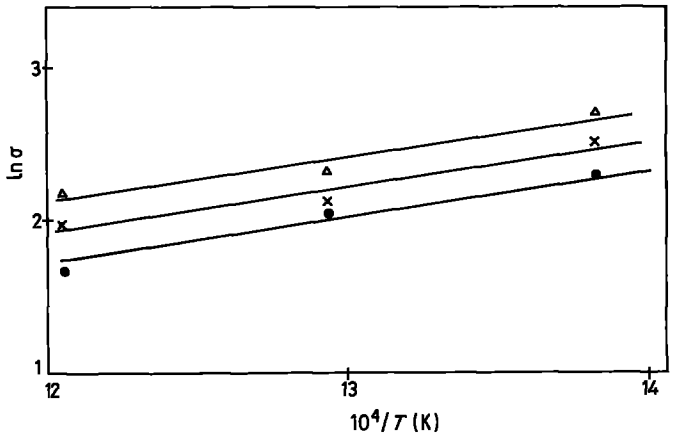

Figure 12 The $\ln \sigma - 1/T$ curves for Alloy 2. Cross-head velocity (●) 0.5, (x) 1, (▲) 2 mm sec^{-1}; $\Delta G = 0.7$ eV.

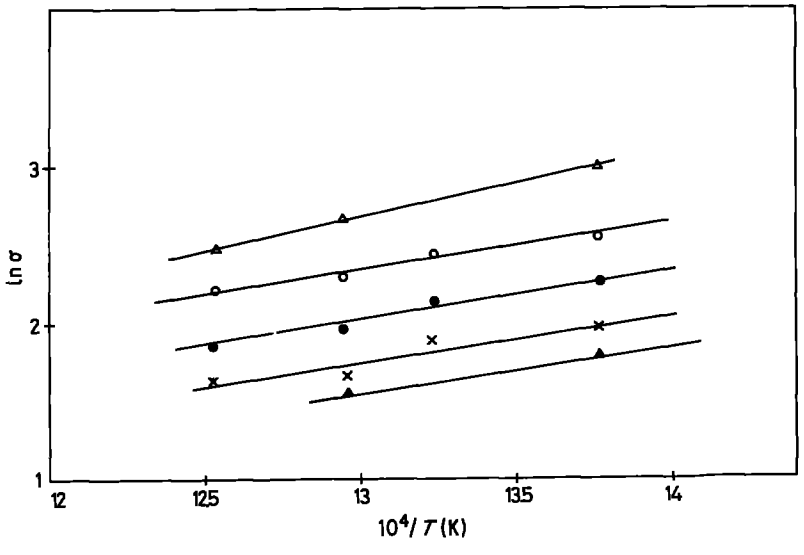

Figure 13 $\ln \sigma - 1/T$ curves for Alloy 3. Cross-head velocity (x) 0.2, (●) 0.5, (○) 1, (▲) 2 mm sec^{-1} at $m \approx 0.4$ and $\Delta G = 0.7$ eV; (△) 3 mm sec^{-1} at $m = 0.3$ and $\Delta G = 1.06$ eV.

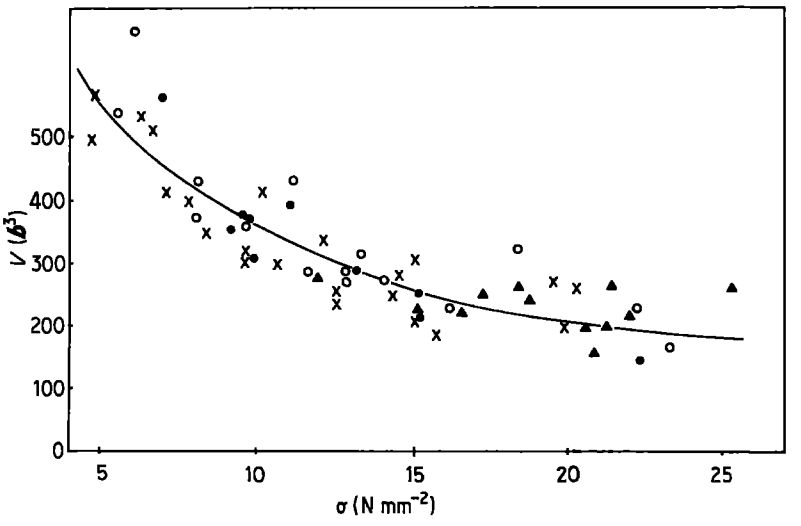

Figure 14 The activation volume (where b, the Burgers vector, = 0.286 nm for aluminium) as a function of stress: (▲) Alloy 1, (●) Alloy 2, (x) Alloy 3, (○) Alloy 4.

characterized by the activation volume

$$V = kT\left(\frac{\partial \ln \dot{\varepsilon}}{\partial \tau}\right)_{T,\varepsilon}$$

where τ is the internal stress. The activation volumes determined on the basis of the strain rate change method are plotted against the stress in Fig. 14. It can be seen that the activation volume first decreases rapidly with stress, after which the decrease is slower. The results agree well with previous ones [1].

5. Conclusions

The superplasticity of the Al–Zn–Mg–Zr alloys can be increased by the addition of iron but it is decreased by simultaneous addition of iron and manganese.

The activation enthalpies obtained indicate that the controlling mechanism of the superplastic deformation is grain-boundary sliding in the alloys investigated.

Acknowledgement

The authors are grateful to Dr Zs. Rajkovits for making the metallographic investigations.

References

1. R. GRIMES, M. J. STOWELL and B. M. WATTS, *Met. Technol.* **3** (1976) 154.
2. B. M. WATTS, M. J. STOWELL, B. L. BAIKIE and D. G. E. OWEN, *Met. Sci.* **10** (1976) 189.
3. T. OKAHASHI and R. ICHIKAWA, *Met. Trans.* **3** (1972) 2300.
4. J. GITTUS, *Res. Mech.* **7** (1985) 125.
5. A. SHAKESHEFF and F. G. PARTRIDGE, *J. Mater. Sci.* **20** (1985) 408.
6. J. W. EDDINGTON, K. N. MELTON and C. P. CUTLER, *Prog. Mater. Sci.* **21** (1976) 61.
7. D. A. WOODFORD, *Trans. Quart. ASM* **62** (1969) 291.
8. F. A. MOHAMED and T. G. LANGDON, *Phys. Status Solidi (a)* **33** (1976) 375.
9. N. L. PETERSON, in Proceedings of the 1979 ASM Materials Science Seminar, Milwaukee, Wisconsin, 15–16 September, 1979 (ASM, Metals Park, Ohio, 1980) p. 209.
10. R. KUTSCHEJ, E. PINK and H. P. STÜWE, *Z. Metallkde* **71** (1980) 666.

Received 25 February
and accepted 28 April 1986